Fluid-structure interaction based algorithms for IOP and corneal material behaviour

Osama Maklad*[1]; Ashkan Eliasy[1]; Kai-Jung Chen[1]; JunJie Wang[2]; Ahmed Abass[1]; Bernardo Teixeira Lopes[1]; Vassilis Theofilis[1]; Ahmed Elsheikh[1, 3, 4]

Affiliation:

[1] School of Engineering, University of Liverpool, Liverpool, L69 3GH, UK

[2] Eye Hospital and the institution of ocular biomechanics, Wenzhou Medical University, Wenzhou, 325027, China

[3] Beijing Advanced Innovation Center for Biomedical Engineering, Beihang University, Beijing, 100083, China

[4] NIHR Biomedical Research Centre for Ophthalmology, Moorfields Eye Hospital NHS Foundation Trust and UCL Institute of Ophthalmology, London, EC1V 9EL, UK

***Corresponding author:**

Email: O.Maklad@liverpool.ac.uk (OM)

Keywords: Ocular biomechanics; Intraocular pressure; Fluid-Structure Interaction (FSI); Corneal material behaviour

Abstract

Purpose: This paper presents and clinically validates two algorithms for estimating intraocular pressure (IOP) and corneal material behaviour using numerical models that consider the fluid-structure interaction between the cornea and the air-puff used in non-contact tonometry.

Methods: A novel multi-physics fluid-structure interaction model of the air-puff test was employed in a parametric numerical study simulating human eyes under air-puff pressure with a wide range of central corneal thickness (CCT=445 to 645 μm), curvature (R=7.4 to 8.4 mm), material stiffness and IOP (10 to 25 mmHg). Models were internally loaded with IOP using a fluid cavity, then externally with air-puff loading simulated using a turbulent computational fluid dynamics model. Corneal dynamic response parameters were extracted and used in development of two algorithms for IOP and corneal material behaviour; fIOP and fSSI, respectively. The two algorithms were validated against clinical corneal dynamic response parameters for 476 healthy participants. The predictions of IOP and corneal material behaviour were tested on how they varied with CCT, R and age.

Results: The present study produced a biomechanically corrected estimation of intraocular pressure (fIOP) and a corneal material stiffness parameter or Stress-Strain Index (fSSI), both of which showed no significant correlation with R ($p > 0.05$) and CCT ($p > 0.05$). Further, fIOP had no significant correlation with age ($p > 0.05$), while fSSI was significantly correlated with age ($p = 0.001$), which was found earlier to be strongly correlated with material stiffness.

Conclusion: The present study introduced two novel algorithms for estimating IOP and biomechanical material behaviour of healthy corneas in-vivo. Consideration of the fluid structure interaction between the cornea and the air puff of non-contact tonometry in developing these algorithms led to improvements in performance compared with bIOP and SSI.

Introduction

It is of increasing clinical importance to quantify the biomechanical properties of the cornea *in vivo*. It would allow better evaluation of corneal ectatic diseases such as keratoconus (KC) [1]–[3] and enable customisation of procedures that interact or interfere mechanically with the cornea including refractive surgeries [4], [5], collagen cross-linking treatment [2], [6], and intrastromal corneal ring segment (ICRS) implantation [7].

The estimation of IOP is an essential measurement in eye examination and crucial in monitoring and treatment of ocular pathologies including glaucoma and ocular hypertension [8]. Therefore, accurate estimation of IOP is highly desirable as the risk of glaucoma progression rises by 11% for every 1 mmHg increase in IOP [9]. The gold standard of IOP measurements is the Goldmann Applanation Tonometer (GAT), which apply a contact force to a central area of the cornea and when this area flattens, it assumes that the external applied pressure equals the internal IOP [10]. This measurement technique makes IOP values sensitive to the natural variations in the central corneal thickness (CCT) and stiffness of the corneal tissue and introduces unacceptable inaccuracies [11]–[13]. This was the main motivation for several attempts to provide IOP estimates that are corrected for corneal biomechanics, such as the Ocular Response Analyzer (ORA Reichert Ophthalmic Instruments, Depew, NY) [14], [15], and the CorVis ST (OCULUS Optikgeräte GmbH; Wetzlar, Germany) [16], [17]. These two devices use a puff of air to applanate the central part of the cornea, where ORA used the cornea's two applanation pressure to reduce association of IOP with CCT and developed the cornea-corrected IOP (IOPcc) estimate, while CorVis-ST uses a high speed Scheimpflug imaging to trace deformation of both the cornea's anterior and posterior profiles under effect of the external air pressure. This high speed imaging technique enabled accurate measurement of corneal thickness, curvature, and corneal deformation patient-specific parameters, which

allowed reliable representation of corneal behaviour in numerical modelling to produce the bIOP estimation algorithm.

Here comes the benefit of the *in vivo* corneal biomechanical characterization in obtaining more accurate estimates of intraocular pressure (IOP). The nonlinearity of corneal tissue behaviour makes the determination of the behaviour *in vivo* quite challenging as the gradient of the stress-strain curve (known as the tangent modulus, E_t) is not constant but increases gradually with applied stress or pressure [19]–[21]. This characteristic creates a difficult challenge with E_t (the measure of stiffness) being dependent on IOP, while the measurement of IOP using tonometry is affected by corneal stiffness. The challenge is to overcome this apparent inter-dependence and produce reliable estimates of both corneal stiffness and IOP.

Progress has been made recently in producing a biomechanically-corrected IOP (bIOP) estimate that is intended to be independent of corneal stiffness [13]. A Stress-Strain Index (SSI) was also developed to estimate the cornea's stress-strain behaviour, and hence E_t at any stress or IOP level [22]. Both bIOP and SSI relied on the dynamic deformation parameters obtained in response to the rapid air-puff of the Corvis ST (OCULUS Optikgeräte GmbH; Wetzlar, Germany) [23]. Earlier studies have shown that bIOP was less influenced by corneal stiffness than both the Goldmann Applanation Tonometer (GAT) and the uncorrected Corvis readings (CVS-IOP) [24]. The studies also found SSI to be almost independent of both central corneal thickness (CCT) and bIOP, while strongly correlated with age.

The present study intended to eliminate an important simplification made in the numerical analyses that led to the development of both bIOP and SSI, namely the assumption that the pressure caused by the air-puff maintained a constant distribution throughout all deformation stages. This assumption is eliminated in the numerical analyses conducted in this study through modelling a 3D air-puff impinging on the cornea using a turbulent computational fluid dynamics (CFD) and Arbitrary Lagrangian-Eulerian (ALE) deforming mesh to couple with the

finite element model of the eye [25], [26]. This method allowed fluid-structure interaction between the air-puff and the eye and enabled the air pressure distribution on the eye to vary in response to corneal deformation in a stepped approach. The corneal deformation predictions obtained with the coupled models were then analysed to develop new algorithms for bIOP and SSI that consider fluid-structure interaction, hence named fIOP and fSSI.

Methods

Numerical models

This study was based on a novel multi-physics, fluid-structure interaction (FSI) model of the air-puff test of the Corvis ST on full eye globes subjected to the internal load of IOP. Details of the numerical model, including, its validation and the used FSI two-way coupling approach with all the co-simulation control parameters and equations were published in our earlier study Maklad et al. [26]. Here, we are giving the most important information, the air-puff was simulated using the turbulent Abaqus/CFD solver (version 6.14-2, Dassault Systèms Simulia Inc., USA) coupled with the finite element model of the eye using an arbitrary Lagrangian-Eulerian (ALE) deforming mesh, Fig 1. A mesh dependence study was performed and Fig S1 shows the apical deformation against number of eye model number of nodes and the pressure on Apex against the air model number of nodes along with the simulation running time, and based on this study the suitable number of elements were selected for every model.

The eye model consisted of 10,000 fifteen-nodded continuum elements (C3D15H) arranged in two layers to keep a consistent aspect ratio of the elements' dimensions, see Fig S2 in the supplementary material. Models of the air domain consisted of 103,680 six-nodded 3D fluid continuum elements (FC3D6) and used Spalart–Allmaras turbulent eddy viscosity model [27], [28] to simulate the turbulence in the air jet. To avoid excessive distortion of the air domain mesh during the coupling process with the eye model, an adaptive Arbitrary Lagrangian–

Eulerian (ALE) deforming mesh was used to improve the stability of the simulation analysis [29]–[31]. The finite element model of the eye was prevented from rigid body motion in the Z-direction (anterior-posterior) at the equatorial nodes. Also, the posterior pole node was restricted in both X and Y directions but were free to move in the Z-direction (anterior-posterior), see Fig S2 in the supplementary material. While the air model domain and its mesh were created over the cornea and a 4 mm ring of the sclera by projecting coordinates of the anterior surface nodes for a distance of 11 mm as this was the distance from the air puff nozzle to the corneal apex. The air jet inlet diameter was set to 2.4 mm, as given by the manufacturers for the nozzle of CorVis-ST, and the maximum air velocity at the inlet was set to 167.8 m/s, which corresponds to a maximum Reynolds number of 2.3×10^4 [26].

Models were generated with an anterior shape factor of 0.82, a limbal radius of 5.85 mm, a sclera external radius of 11.5 mm and the thickness regional variation reported in earlier studies [19], [20], [22], [32]. The eye models adopted the material stress-strain behaviour patterns that were found in earlier experimental studies to correlate with age within the range 30-100 years [22], [32], [33]. They were as presented in Equation 1 for corneal material, and Equation 2 for anterior, equatorial and posterior sclera.

$$\sigma = (35\times10^{-9}age^2 + 1.4\times10^{-6}age + 1.03\times10^{-3}) \times \left[e^{(0.0013age^2+0.013age+99)\varepsilon} - 1\right] \quad (1)$$

$$\sigma = \frac{2\mu}{\alpha}.\left((\varepsilon+1)^{\alpha-1} - (\varepsilon+1)^{-(1+\frac{\alpha}{2})}\right), \quad (2)$$

$$where \begin{cases} \mu = 1.26\ age + 0.94, \alpha = 20.1\ age + 19.8, & for\ anterior\ sclera \\ \mu = 0.85\ age + 0.42, \alpha = 12.6\ age + 34.16, & for\ equatorial\ sclera \\ \mu = 0.22\ e^{1.19\ age}, \alpha = 53.02, & for\ posterior\ sclera \end{cases}$$

In Equations 1 and 2, σ is the stress in MPa and age is in years. Similar to the SSI [22], fSSI was set to 1.0 for a stress-strain relationship that corresponded to the mean behaviour found experimentally for corneas aged 50 years [33]. The patient's age is a direct parameter in changing corneal material stiffness which is a crucial input parameter in the material definition for the finite element model of the eye according to the experimental study conducted by Elsheikh et al. [33]. Increases and decreases in fSSI relative to 1.0 corresponded to stress-strain relationships for which E_t at any stress level grew or reduced by the same change in fSSI. With this principle in mind, the stress-strain behaviour in the cornea that corresponded to any age could be converted into an fSSI value.

The eye models were built using a bespoke software package generated in MATLAB® (Natick, Massachusetts, USA). The analysis started by finding the stress-free geometry (under zero IOP) for each eye model using an iterative approach reported earlier [34] . The coupled models were then subjected to IOP followed by Corvis air pressure, and the resulting deformation across the eye globe was stored for later analysis. Another bespoke MATLAB code was used to extract and record the corneal response parameters, example is shown in Fig 2, along with the models' input parameters [25], [35], [36]. Fig 2(a) shows the peak point location at highest corneal concavity, at which stage the peak distance was calculated as the distance between the two corneal peaks. This calculation started with fitting the corneal curve to a polynomial, identifying the points with maximum Z-coordinate and finding the distance from corneal centre (X-coordinate). Fig 2(b) shows the method used to determine the time to first applanation, and the corresponding air pressure and apical deformation. This was done by calculating the first and second derivatives of the corneal profile at apex for every time step. When the derivatives reach a value of zero, indicating a flattened corneal surface, this behaviour stage was considered the point of first applanation. On the other hand, Fig 2(c) illustrates how the applanation length is estimated by calculating the difference between the Z-coordinates at apex and neighbouring

points. Where the difference in Z-coordinate exceeded 0.01 mm was considered the end of the peak length.A parametric study was carried out to gauge the influence of model input parameters on corneal biomechanical parameters as a response to the air-puff. This was performed with wide ranges of central corneal thickness, CCT, between 445 and 645 μm, IOP between 10 and 25 mmHg, central corneal curvature, R, between 7.4 and 8.4 mm, and corneal material stiffness coefficient, μ(stiffness parameter), between 0.0422 and 0.1082. The influence matrix of each parameter on corneal response parameters is shown in Fig S3 in supplementary material and all Pearson's correlation values are shown in Table S1, which was published in our earlier study, Maklad et al. [26].

fIOP and fSSI algorithms

The numerical models had IOP, CCT, R and age as input parameters, and the output was corneal deformation profiles that resulted in response parameters including, most notably, peak distance, first applanation deformation amplitude, first applanation length, highest concavity deformation amplitude and highest concavity radius, Fig 2. Analysis of the input and output parameters allowed the development of two relationships for fIOP as a function of CCT, R, age, and corneal deformation parameter with strong correlation with true IOP and fSSI as a function of CCT, fIOP, and corneal deformation parameter with strong correlation with material stiffness

The significance of the correlations of corneal deformation parameters with IOP and age was assessed in SPSS Version 24 (IBM Corp., USA) and confirmed with a probability value, $p < 0.05$ or a high Pearson's correlation coefficient (r). For each of the parameters for which significant correlation was confirmed, an exercise was conducted to determine the lowest possible polynomial order that should be adopted in the fIOP equation based on the lowest route mean square error (RMSE). The objective function adopted took the form:

$$Objective\ function = \min RMS = min\sqrt{\frac{1}{N}\sum_{i=1}^{N}(fIOP_i - true\_IOP_i)^2}, \quad (3)$$

Where *RMS* is the root mean square of the error, *N* is the number of eye models, and *true_IOP* is the value set in the numerical models.

The development of the fSSI followed a similar route and the objective function used took the form:

$$Objective\ function = \min RMS = min\sqrt{\frac{1}{N}\sum_{i=1}^{N}(fSSI - SSI)^2}, \quad (4)$$

Where *RMS* is the root mean square of the error, *N* is the number of eye models, and *SSI* is the value set in the numerical models.

Clinical validation

In this retrospective study, we reviewed the Corvis data of right and left eyes of 476 healthy participants from the Vincieye Clinic in Milan, Italy and Rio de Janeiro Corneal Tomography and Biomechanics Study Group, Brazil. The participants had an age range between 10 to 87 years, CCT between 455 and 630 µm and IOP between 9 and 25 mmHg, Table 1. The data included the maximum deformation, first applanation pressure, first applanation time, highest concavity radius, spatial and temporal corneal deformation. The Institutional review board of the University of Liverpool ruled that approval was not obligatory for this record review study. However, the ethical standards set out in the 1964 Declaration of Helsinki and their revision in 2013 were observed and all patients provided informed written consent before using their de-identified data in research.

The data was used to assess whether, as expected, fIOP was independent of CCT, age and R. Similarly, fSSI's independence of CCT and IOP, and correlation with age were assessed using

the same dataset. This exercise also enabled comparing fIOP against bIOP, and fSSI against SSI, in order to check whether the improved modelling adopted in this study, through consideration of the fluid-structure interaction, had led to improvements in IOP and material stiffness estimates.

Results

Air pressure distribution

To demonstrate the effect of fluid-structure interaction on the value and distribution of air pressure acting on the cornea, the results of two typical simulations are first compared; one assuming a rigid cornea that does not change shape under air pressure and another with FSI coupling between the air domain and the finite element model of the eye. Fig 3(a-c) shows the two pressure distributions as actual and normalised values at times T=8 and 16 ms and demonstrate a small reduction in apical pressure of around 6.3% at 16 ms when FSI was considered. Additionally, Fig 3(d) shows how the temporal pressure profile changes from one model to another due to changes in the corneal biomechanical parameters. The means of these differences were small 3.4% at T=8 ms and increased to 8.4% at 16 ms. Fig S4 in supplementary material shows the air velocity and pressure coefficient distribution on the cornea explaining how the dynamic pressure converts into static pressure on the cornea and why there is a negative pressure region at 2 mm from cornea apex.

Correlation analysis

A bivariate correlation analysis was carried out between each of the model's output corneal response parameters and the four main input parameters (IOP, CCT, R and age – representing corneal stiffness) and the influence matrix of each parameter on corneal response parameters is shown in Fig S2 in the supplementary material. The full correlation analysis and comparison

with the clinical corneal response parameters are available in our earlier study, Maklad et al. [25], [26], which revealed that the first applanation pressure (AP1), and the highest concavity radius (R_{HC}) were the highest correlated parameters to IOP (r= 0.736 and 0.624, respectively, and p< 0.001). For this reason, AP1 and R_{HC}, along with CCT, R and age were included in the fIOP equation. On the other hand, the stiffness parameter at highest concavity (SP- HC) was the most associated response parameters to corneal material change (r= 0.442, p< 0.01), and was therefore included with CCT and fIOP in the corneal material estimation algorithm.

fIOP equation

Using the least-squares method, the fIOP equation took the form:

$$fIOP = C_{AP1} \times C_{CCT-age} \times C_R \times C_{R_{HC}} + C \quad (5)$$

where

$$C_{AP1} = (-0.005 \times AP1 + 0.19)$$

$$C_{CCT-age} = (0.011 \times CCT^3\mu^3 - 0.002 \times CCT^3\mu^2 + 9.17 \times CCT^3\mu + 8.34 \times CCT^3$$
$$-6.3 \times CCT^2\mu^3 + 1.16 \times CCT^2\mu^2 - 0.05 \times CCT^2\mu - 0.003 \times CCT^2$$
$$+0.76 \times CCT\mu^3 + 5.67 \times CCT\mu^2 - 4.87 \times CCT\mu + 1.73 \times CCT$$
$$-0.55 \times \mu^3 + 0.76 \times \mu^2 + 1.82 \times \mu + 4.09)$$

$$\mu = (0.076\, e^{0.536\, age})$$

$$C_R = (0.045 \times R - 0.213 \times 10^{-3})$$

$$C_{R_{HC}} = (-0.0008 \times R_{HC} - 0.68)$$

$$C = 9.36$$

In this equation, fIOP and AP1 were in mmHg, CCT in microns, R and R_{HC} in mm and age in years. With this equation form, the RMS error was 4.5%.

Validation of fIOP using clinical data

Fig 4 presents an analysis of the association of fIOP, the previously developed bIOP, and the uncorrected Corvis IOP readings (CVS-IOP) with CCT, age and corneal curvature. The results show similar performance of fIOP with that of bIOP in reducing the association CVS-IOP with CCT. The figure also demonstrates better performance with fIOP than with bIOP in reducing the association of CVS-IOP with both age and R.

Material stiffness (fSSI) algorithm

Similar to the fIOP equation, the fSSI algorithm was developed using the least-squares method, leading to the following form:

$$fSSI = \begin{cases} 0.5,\ for\ Ln(SP-HC) = 0.026 + 1.83 \times (fIOP/20) + 2.26 \times (CCT/545) \\ 1.0,\ for\ Ln(SP-HC) = 0.68 + 1.44 \times (fIOP/20) + 2.36 \times (CCT/545) \\ 1.5,\ for\ Ln(SP-HC) = 0.85 + 1.49 \times (fIOP/20) + 2.35 \times (CCT/545) \\ 2.0,\ for\ Ln(SP-HC) = 1.11 + 1.02 \times (fIOP/20) + 2.55 \times (CCT/545) \\ 3.0,\ for\ Ln(SP-HC) = 1.33 + 1.05 \times (fIOP/20) + 2.54 \times (CCT/545) \end{cases} \quad (6)$$

where fIOP is in mmHg and CCT is in microns. For intermediate values of $Ln(SP-HC)$, interpolation between the values of fSSI could be performed. With this equation form, the RMS error was 8.83 %.

Validation of fSSI against clinical data

As additional validation of fSSI, its correlation with CCT, age and fIOP is assessed. Weak correlation with CCT and fIOP would be a sign of success along with positive correlation with age (where earlier evidence pointed at tissue stiffening with ageing [32], [33]). The results shown in Fig 5 present better performance than SSI in maintaining weak correlation with CCT

and IOP. Meanwhile, the correlation of fSSI with age was stronger than for SSI (r^2 = 0.415 vs 0.191). Moreover, as a validation against clinical corneal deformation profiles, six cases are presented in Fig S5 in terms of the spatial corneal deformations and temporal apical deformation.

Discussion

The main objective of this study is to investigate the influence of considering the fluid-structure interaction between the air puff and the cornea on the reliability of methods to estimate the biomechanically-corrected IOP and the corneal material behaviour. IOP is interlinked with material stiffness in a complex loop as the measurement of IOP in tonometry is commonly influenced by corneal stiffness, while the tangent modulus (a measure of stiffness) is known to increase with the level of IOP [22], [37]. The challenge to provide estimations of IOP and corneal stiffness that are independent of each other was dealt with in the present study using numerical modelling and employing the results to build algorithms to estimate fIOP and corneal material index fSSI. These algorithms included a number of Corvis deformation parameters, namely the first applanation pressure (AP1) and the highest concavity radius (R_{HC}) in the fIOP equation, and the stiffness parameter (SP-HC) in the fSSI equation.

This challenge was addressed in earlier studies in the development of bIOP and SSI [22], [24], [38], and this study aimed to use more representative numerical modelling that considered the fluid-structure interaction between the air puff and the cornea. With this new model, which employed the arbitrary Lagrangian-Eulerian deforming mesh, small changes could be observed in the temporal and spatial pressure distribution profiles on the cornea, and these changes were dependent on the eye's geometric features and material stiffness. The FSI effect was more evident when the cornea's deformation was high as in cases small CCT or low IOP.

Consideration of these pressure distribution profiles in the development of an algorithm to estimate fIOP resulted in better performance compared to the bIOP in reducing the association of IOP measurements with both age and R, but maintained similar low correlation with CCT. Consideration of the pressure distribution profiles in developing the fSSI algorithm resulted in similar improvements compared with the SSI with slightly weaker dependence on CCT and fIOP while maintaining similar correlation with age.

The development of these algorithms could benefit clinical practice in providing biomechanically-corrected IOP measurements to improve glaucoma diagnosis and management. They can also help in keratoconus detection via increasing the effectiveness of existing biomechanical indices such as the Tomography and Biomechanical Index (TBI) [23] and the Corvis Biomechanical Index (CBI) [39], especially that the FSI effect is more evident in soft corneas such as those with keratoconus [1], [39], [40].

There were some limitations in the current study, which are important to note. The eye model employed in the study did not include soft tissue filling the orbital space and surrounding the eye which gives the eye freedom to move backward. Moreover, clinically, the air puff shooting direction can be sometimes at an angle from the eye axis and a modification for the mesh was done to apply the air puff at an angle, but the problem is that it's not known how the air puff will hit the cornea in order to make a global correction which fits with all patients. Finally, the current study concentrated on developing the numerical model and the algorithms for healthy eyes and the next step is to extend the study for keratoconic eyes before and after crosslinking.

In conclusion, we developed novel algorithms for IOP and corneal material estimation in-vivo for healthy corneas by considering the fluid-structure interaction between the air-puff of the Corvis ST tonometer and the eye globe. The algorithms demonstrated slightly better performance than bIOP and SSI, contributing further to the reliability of these algorithms and assisting their application in clinical practice.

Acknowledgement

We would like to acknowledge OCULUS Optikgeräte GmbH for their support with CorVis-ST. Great appreciation to the Vincieye Clinic in Milan, Italy and Rio de Janeiro Corneal Tomography and Biomechanics Study Group, Brazil for permission to work on the clinical data provided.

Supplementary Material

All relevant data are within the manuscript and its supplementary material file; Fig S1: Mesh sensitivity analysis for the FSI model; Fig S2: Fluid-structure interaction (FSI) model of the air-puff test of the Corvis ST on full eye globe; Fig S3 Influence matrices of changing model input parameters on corneal response parameters; Fig S4: Analysis of air velocity, pressure coefficient and corneal deformation magnitude at the cornea; Files F2, F3: Fluid–structure interaction coupled analysis model input files. File F4 is the parametric study database.

Author Contributions

Conceptualization, Ah.E.; Data curation, O.M., K.-J.C. and JJ.W.; Formal analysis, O.M.; Project administration, O.M. and As.E.; Resources, Ah.E.; Software, O.M.; Supervision, V.T. and Ah.E.; Validation, O.M., B.TL., JJ.W. Ah.A., V.T. and Ah.E.; Visualization, As.E., K.-J.C. and V.T.; Writing – original draft, O.M.; Writing – review & editing, O.M., As.E., B.TL., Ah.A.,V.T. and Ah.E.**.** All authors reviewed the paper and gave final approval.

Ethical statement

The Institutional review board of the University of Liverpool ruled that approval was not obligatory for this record review study. However, the ethical standards set out in the 1964

Declaration of Helsinki and their revision in 2013 were observed and all patients provided informed written consent before using their de-identified data in research.

Conflicts of Interest

Prof. Elsheikh is a consultant for OCULUS Optikgeräte GmbH. None of the remaining authors have financial disclosures or personal interests in the work reported in this paper.

Funding statement

No funding received to support this research.

References

[1] C. Ye, M. Yu, G. Lai, and V. Jhanji, "Variability of corneal deformation response in normal and keratoconic eyes," *Optom. Vis. Sci.*, vol. 92, no. 7, pp. e149–e153, 2015.
[2] S. H. Chang *et al.*, "The relationship between mechanical properties, ultrastructural changes, and intrafibrillar bond formation in corneal UVA/riboflavin cross-linking treatment for keratoconus," *J. Refract. Surg.*, vol. 34, no. 4, pp. 264–272, 2018.
[3] F. Bao, B. Geraghty, Q. Wang, and A. Elsheikh, "Consideration of corneal biomechanics in the diagnosis and management of keratoconus: is it important?," *Eye Vis.*, vol. 3, no. 1, p. 18, Dec. 2016.
[4] A. Sorsby, "The nature of refractive errors," *Br. Med. Bull.*, vol. 9, no. 1, pp. 22–23, 1953.
[5] "Surgery for Refractive Errors," *Lancet*, vol. 325, no. 8426, pp. 435–436, 1985.
[6] E. Spoerl, N. Terai, F. Scholz, F. Raiskup, and L. E. Pillunat, "Detection of Biomechanical Changes After Corneal Cross-Linking Using Ocular Response Analyzer Software," *J. Refract. Surg.*, vol. 27, no. 6, pp. 452–457, Jun. 2011.
[7] C. J. Roberts and W. J. Dupps, "Biomechanics of corneal ectasia and biomechanical treatments," *Journal of Cataract and Refractive Surgery*, vol. 40, no. 6. pp. 991–998, 2014.
[8] R. L. Stamper, "A history of intraocular pressure and its measurement.," *Optom. Vis. Sci.*, vol. 88, no. 1, pp. E16-28, Jan. 2011.
[9] B. Bengtsson, M. C. Leske, L. Hyman, and A. Heijl, "Fluctuation of Intraocular Pressure and Glaucoma Progression in the Early Manifest Glaucoma Trial," *Ophthalmology*, vol. 114, no. 2, pp. 205–209, Feb. 2007.
[10] H. Goldmann and T. Schmidt, "Über Applanationstonometrie," *Ophthalmologica*, vol. 134, no. 4, pp. 221–242, Oct. 1957.
[11] L. V. Hemdon, S. A. Choudhri, T. Cox, K. F. Damji, M. Brace Shields, and R. Rand Allingham, "Central corneal thickness in normal, glaucomatous, and ocular

hypertensive eyes," *Arch. Ophthalmol.*, vol. 115, no. 9, pp. 1137–1141, Sep. 1997.
[12] J. Liu and C. J. Roberts, "Influence of corneal biomechanical properties on intraocular pressure measurement: Quantitative analysis," *J. Cataract Refract. Surg.*, vol. 31, no. 1, pp. 146–155, 2005.
[13] A. Eliasy *et al.*, "Ex-vivo experimental validation of biomechanically-corrected intraocular pressure measurements on human eyes using the CorVis ST," *Exp. Eye Res.*, vol. 175, pp. 98–102, Oct. 2018.
[14] D. Luce, "Air–Jet Temporal and Spatial Pressure Properties of the Reichert Ocular Response Analyzer (ORA)," *Invest. Ophthalmol. Vis. Sci.*, vol. 46, no. 13, pp. 5009–5009, May 2005.
[15] R. Montard *et al.*, "Ocular Response Analyzer: Étude de fiabilité et de corrélation sur des yeux normaux," *J. Fr. Ophtalmol.*, vol. 30, no. 10, pp. 978–984, Dec. 2007.
[16] R. Vinciguerra *et al.*, "Influence of Pachymetry and Intraocular Pressure on Dynamic Corneal Response Parameters in Healthy Patients," *J. Refract. Surg.*, vol. 32, no. 8, pp. 550–561, Aug. 2016.
[17] A. A. Joda, M. M. S. Shervin, D. Kook, and A. Elsheikh, "Development and validation of a correction equation for Corvis tonometry," *Comput. Methods Biomech. Biomed. Engin.*, vol. 19, no. 9, pp. 943–953, 2015.
[18] A. Elsheikh, C. W. McMonnies, C. Whitford, and G. C. Boneham, "In vivo study of corneal responses to increased intraocular pressure loading," *Eye Vis.*, vol. 2, no. 1, p. 20, 2015.
[19] A. Kotecha, A. Elsheikh, C. R. Roberts, H. Zhu, and D. F. Garway-Heath, "Corneal thickness- and age-related biomechanical properties of the cornea measured with the ocular response analyzer," *Investig. Ophthalmol. Vis. Sci.*, vol. 47, no. 12, pp. 5337–5347, 2006.
[20] A. Elsheikh, D. Wang, and D. Pye, "Determination of the modulus of elasticity of the human cornea.," *J. Refract. Surg.*, vol. 23, no. 8, pp. 808–818, 2007.
[21] A. Elsheikh, "Finite Element Modeling of Corneal Biomechanical Behavior," *J. Refract. Surg.*, vol. 26, no. 4, pp. 289–300, 2010.
[22] A. Eliasy *et al.*, "Determination of Corneal Biomechanical Behavior in-vivo for Healthy Eyes Using CorVis ST Tonometry: Stress-Strain Index," *Front. Bioeng. Biotechnol.*, vol. 7, p. 105, May 2019.
[23] R. Ambrósio *et al.*, "Integration of Scheimpflug-Based Corneal Tomography and Biomechanical Assessments for Enhancing Ectasia Detection," *J. Refract. Surg.*, vol. 33, no. 7, pp. 434–443, 2017.
[24] A. Eliasy *et al.*, "Ex-vivo experimental validation of biomechanically-corrected intraocular pressure measurements on human eyes using the CorVis ST," *Exp. Eye Res.*, vol. 175, no. June, pp. 98–102, 2018.
[25] O. Maklad, "Influence of Fluid Structure Interaction on Human Eye Biomechanics Under Air Puff Non-contact Tonometry," *Ph. D. Thesis*, no. uk.bl.ethos.778526, 2019.
[26] O. Maklad, A. Eliasy, K. J. Chen, V. Theofilis, and A. Elsheikh, "Simulation of air puff tonometry test using arbitrary lagrangian–eulerian (ALE) deforming mesh for corneal material characterisation," *Int. J. Environ. Res. Public Health*, vol. 17, p. 54, 2020.
[27] NASA, "Turbulence Modeling Resource: The Spalart-allmaras Turbulence," *Recherche*, 2011. [Online]. Available: https://turbmodels.larc.nasa.gov/.
[28] H. K. Versteeg and W. Malalasekera, "An Introduction to Computational Fluid Dynamics - The Finite Volume Method," *Fluid flow handbook. McGraw-Hill …*. 1995.
[29] M. Kcharik, R. Liska, P. Váchal, and M. Shashkov, "Arbitrary Lagrangian-Eulerian

(ALE) Method in compressible fluid dynamics," *Programs Algorithms Numer. Math.*, pp. 178–183, 2006.
[30] J. Hron and S. Turek, "A Monolithic FEM/Multigrid Solver for an ALE Formulation of Fluid-Structure Interaction with Applications in Biomechanics," in *Fluid-Structure Interaction*, Berlin, Heidelberg: Springer Berlin Heidelberg, 2006, pp. 146–170.
[31] J. Donea, A. Huerta, J.-P. Ponthot, and A. Rodríguez-Ferran, "Arbitrary Lagrangian-Eulerian Methods," in *Encyclopedia of Computational Mechanics Second Edition*, 2017, pp. 1–23.
[32] A. Elsheikh, B. Geraghty, D. Alhasso, J. Knappett, M. Campanelli, and P. Rama, "Regional variation in the biomechanical properties of the human sclera," *Exp. Eye Res.*, vol. 90, pp. 624–633, 2010.
[33] A. Elsheikh, B. Geraghty, P. Rama, M. Campanelli, and K. M. Meek, "Characterization of age-related variation in corneal biomechanical properties," *J. R. Soc. Interface*, vol. 7, no. 51, pp. 1475–1485, 2010.
[34] A. Elsheikh, C. Whitford, R. Hamarashid, W. Kassem, A. Joda, and P. Büchler, "Stress free configuration of the human eye," *Med. Eng. Phys.*, vol. 35, no. 2, pp. 211–216, Feb. 2013.
[35] M. Jędzierowska and R. Koprowski, "Novel dynamic corneal response parameters in a practice use: a critical review," *Biomed. Eng. Online*, vol. 18, no. 1, p. 17, Dec. 2019.
[36] J. L. C. J. ROBERTS, *CORNEAL BIOMECHANICS: From Theory to Practice*. KUGLER PUBLICATIONS, 2017.
[37] E. M., A. Elsheikh, and P. Gunvant, "Tonometry – Past, Present and Future," *Glaucoma - Curr. Clin. Res. Asp.*, no. May, 2011.
[38] K.-J. Chen *et al.*, "Development and validation of a new intraocular pressure estimate for patients with soft corneas," *J. Cataract Refract. Surg.*, vol. 45, no. 9, pp. 1316–1323, Sep. 2019.
[39] R. Vinciguerra *et al.*, "Detection of Keratoconus With a New Biomechanical Index," *J. Refract. Surg.*, vol. 32, no. 12, pp. 803–810, 2016.
[40] T. T. Andreassen, A. Hjorth Simonsen, and H. Oxlund, "Biomechanical properties of keratoconus and normal corneas," *Exp. Eye Res.*, vol. 31, no. 4, pp. 435–441, 1980.

Tables

Table 1: Clinical dataset used in the validation of fIOP and cornea material characterisation algorithms

Datasets	Participants	Age (years)	CCT (μm)	CVS-IOP (mmHg)
Dataset 1 (Milan)	225	38 ± 17.2 (7–91)	543 ± 31.5 (458–635)	15.7 ± 2.35 (11–25)
Dataset 2 (Rio)	251	43 ± 16.5 (8–87)	539 ± 33.2 (454–629)	14.8 ± 3.06 (6–34)

471 **Figures**

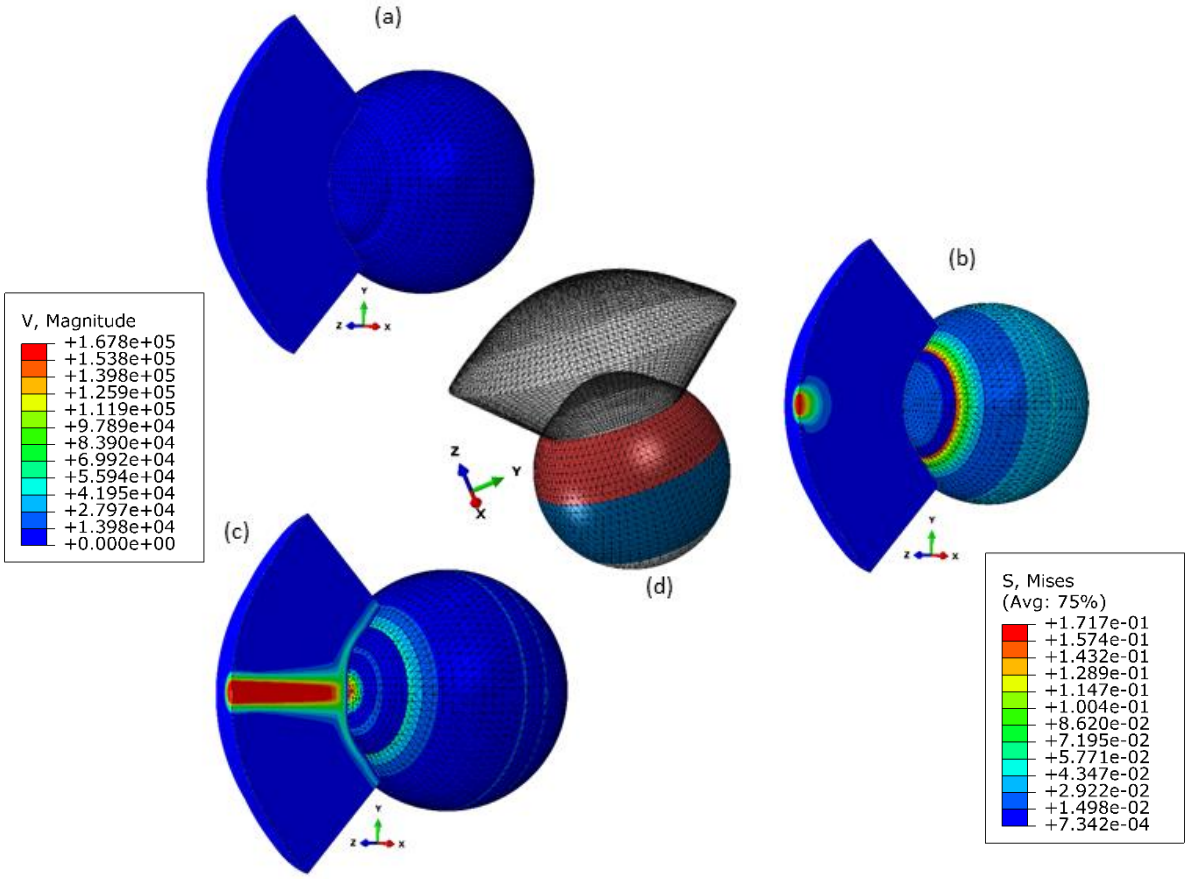

Figure 1: Fluid structure interaction (FSI) model of the air puff test (a) Stress-free configuration, (b) model after applying internal IOP, (c) Model at highest concavity and (d) is showing the different material sections in the eye model. The legend on the left is the magnitude of the air velocity in mm/s from the CFD model and the legend on the right is the magnitude of Von-Mises stress from the finite element model of the eye.

472

473

474

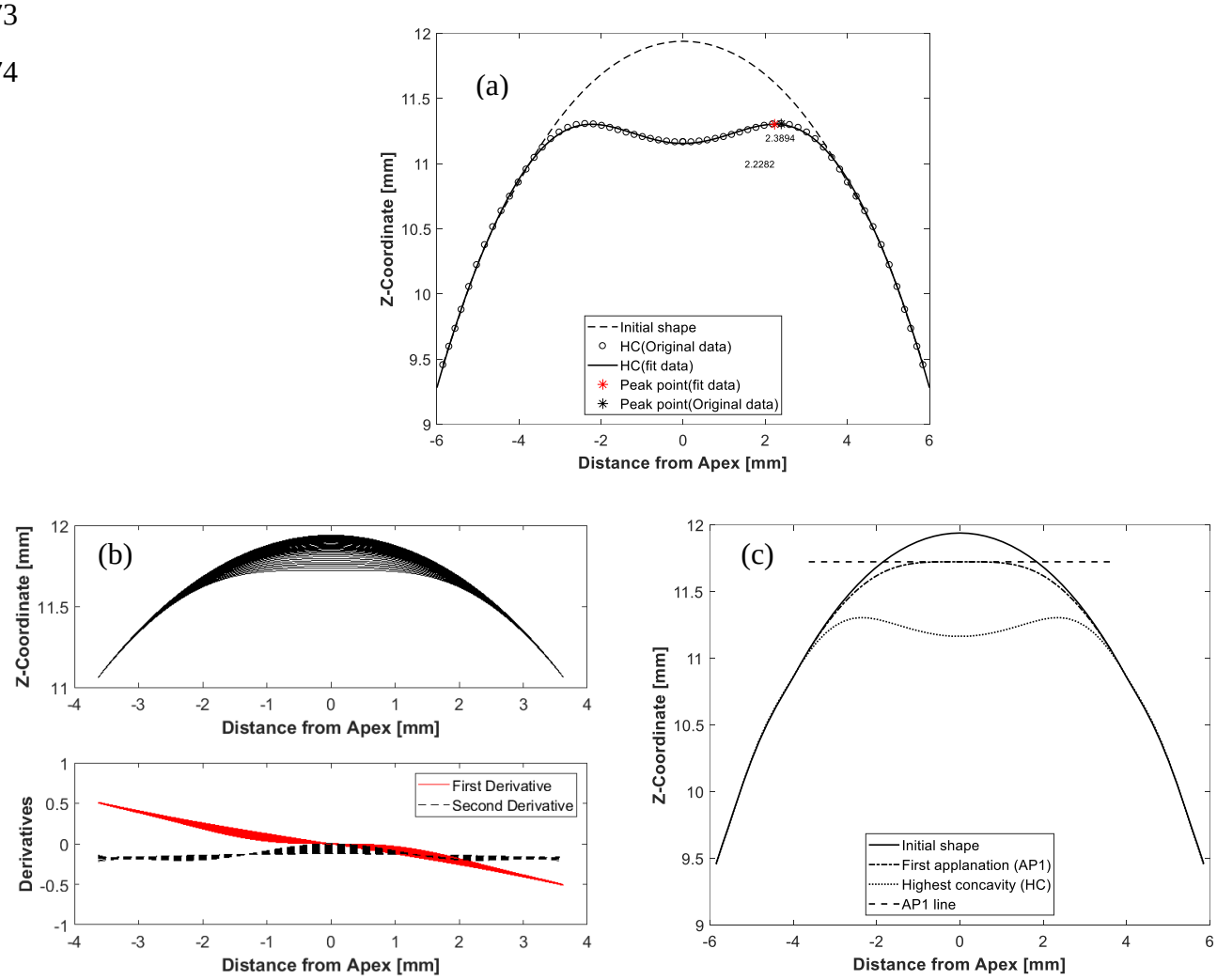

Figure 2: Example results of a typical analysis showing corneal deformation parameters from the numerical model including (a) peak point location at highest corneal concavity to calculate peak distance, which is the distance between the two corneal peaks, (b) first applanation moment determined by using first and second derivatives of corneal profiles over the 7 mm diameter central zone, and (c) applanation length by calculating the difference between Apex Z-coordinate and its neigbouring points until a tolerance of 0.01 is broken

475

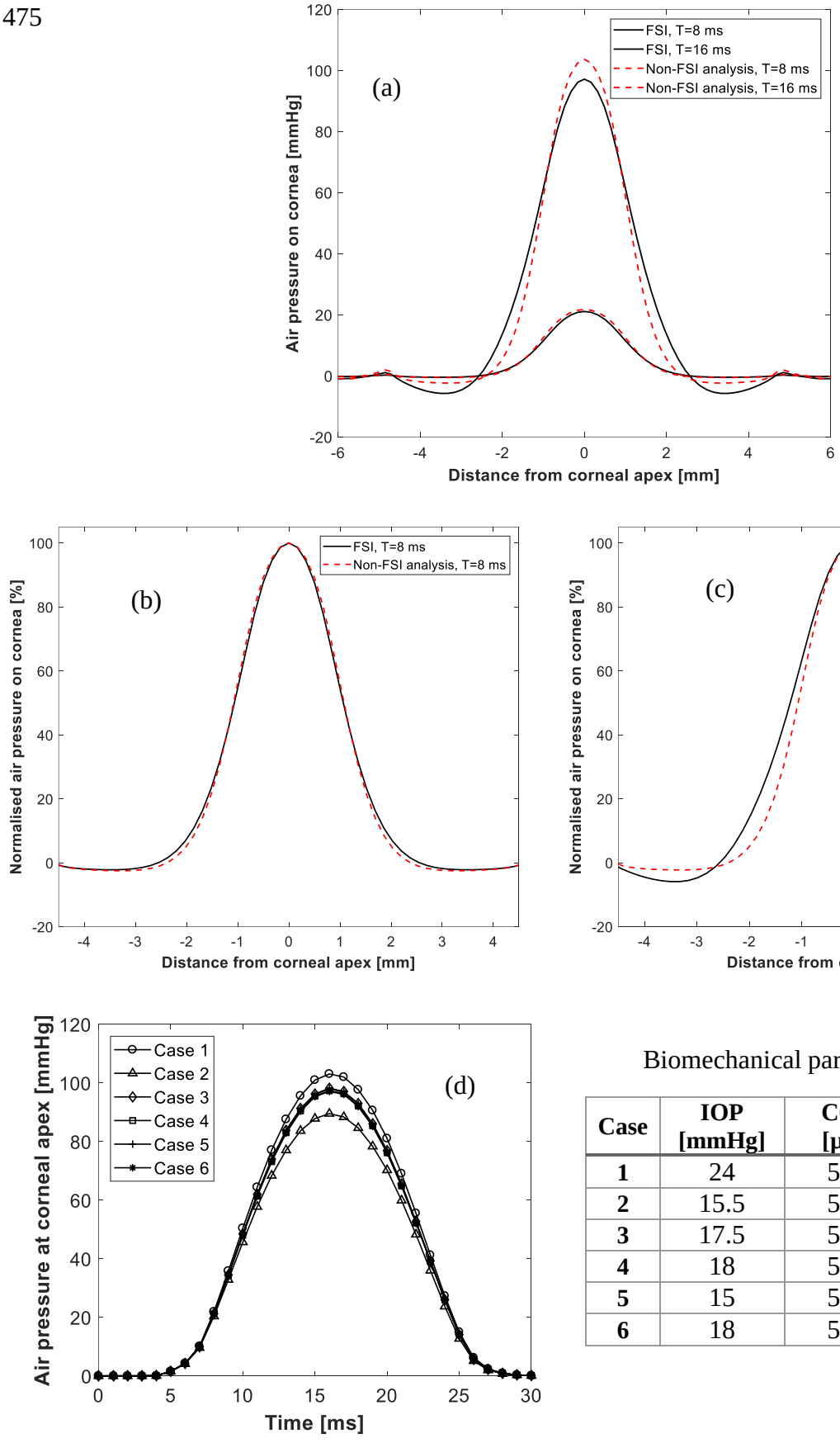

Biomechanical parameters of the six cases

Case	IOP [mmHg]	CCT [µm]	R [mm]	Age [Years]	Gender
1	24	582	6.95	39	F
2	15.5	587	7.60	30	M
3	17.5	560	7.61	73	F
4	18	579	7.15	54	F
5	15	548	7.48	63	M
6	18	550	8.03	62	M

Figure 3 Predicted pressure distribution on the cornea with and without FSI analysis in (a) actual values, and (b, c) normalised values at 8 ms and 16 ms after start of pressure application. Temporal pressure profiles for 6 different models are shown in (d). Details of the 6 cases are given in table.

(a) Central corneal thickness (CCT)

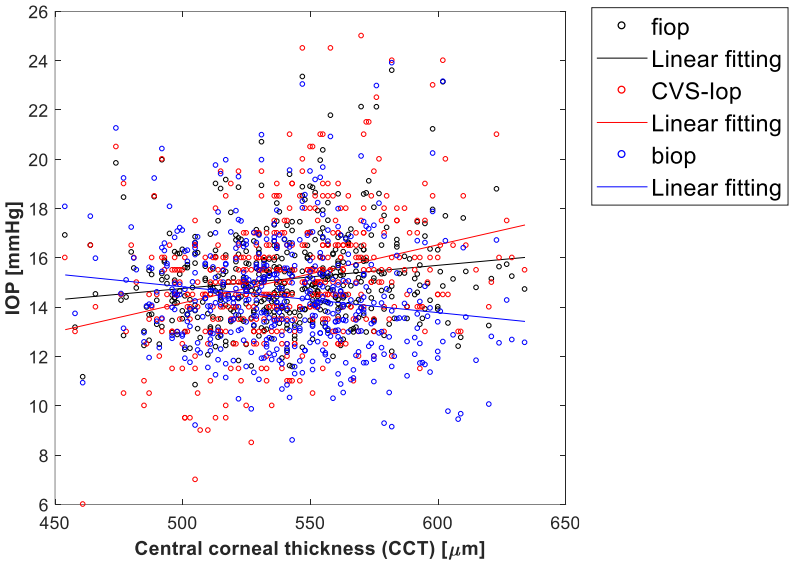

$fIOP = 0.0094\ CCT + 10.1$

$r^2 = 0.026$

$CVS - IOP = 0.0236\ CCT + 2.4$

$r^2 = 0.0884$

$bIOP = -0.011\ CCT + 20.1$

$r^2 = 0.0219$

(b) Age

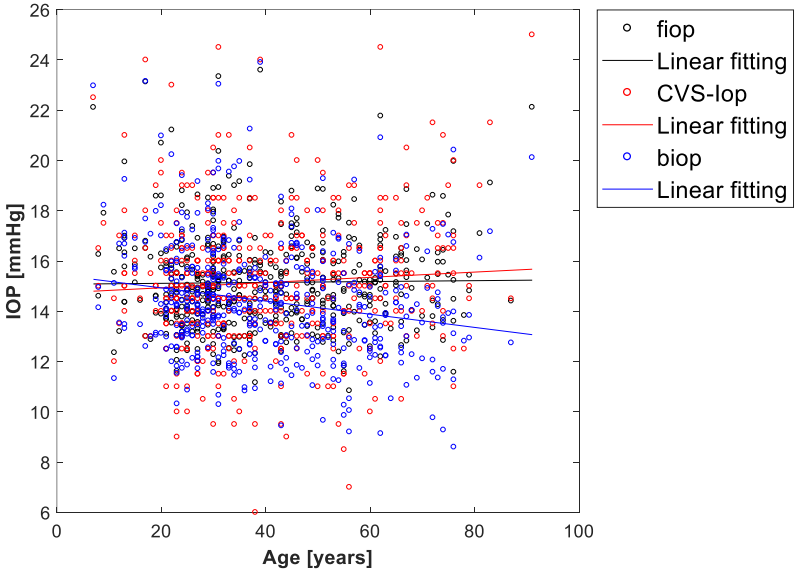

$fIOP = 0.0018\ age + 15.1$

$r^2 = 0.0003$

$CVS - IOP = 0.01\ age + 14.7$

$r^2 = 0.0047$

$bIOP = 0.026\ age + 15.5$

$r^2 = 0.0376$

(c) Corneal apical radius (R)

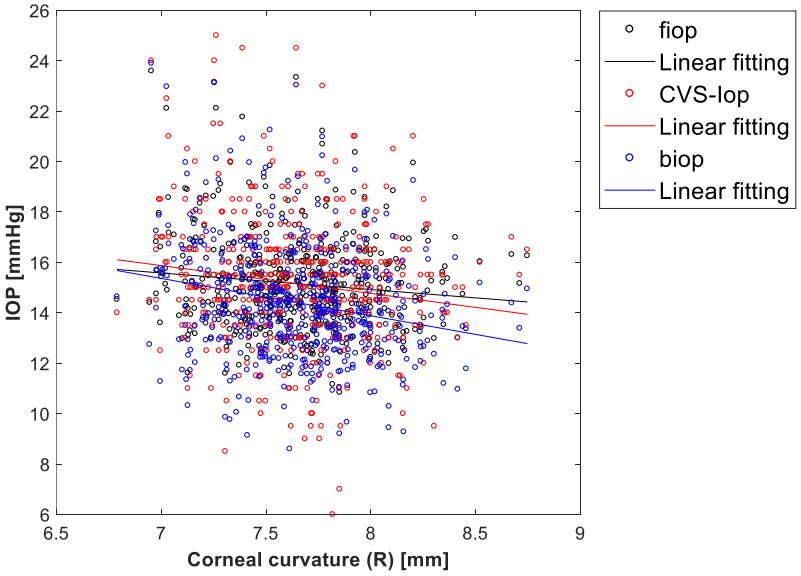

$fIOP = -0.658\ R + 20.19$

$r^2 = 0.0137$

$CVS - IOP = -1.11\ R + 23.6$

$r^2 = 0.0208$

$bIOP = -1.48\ R + 25.7$

$r^2 = 0.0469$

Figure 4: Association of fIOP, CorVis, and bIOP values with (a) central corneal thickness, (b) age, and (c) corneal apical radius

(a) Central corneal thickness (CCT)

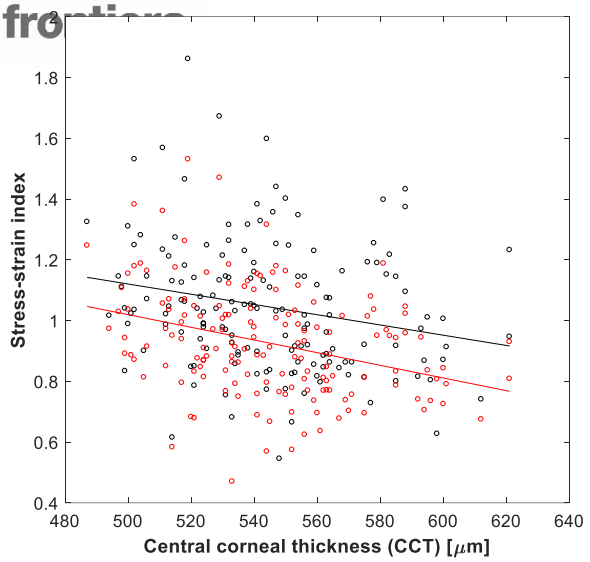

$$fSSI = -0.0017\ CCT + 1.96$$

$$r^2 = 0.0498$$

$$SSI = -0.0021\ CCT + 2.06$$

$$r^2 = 0.1112$$

(b) Age

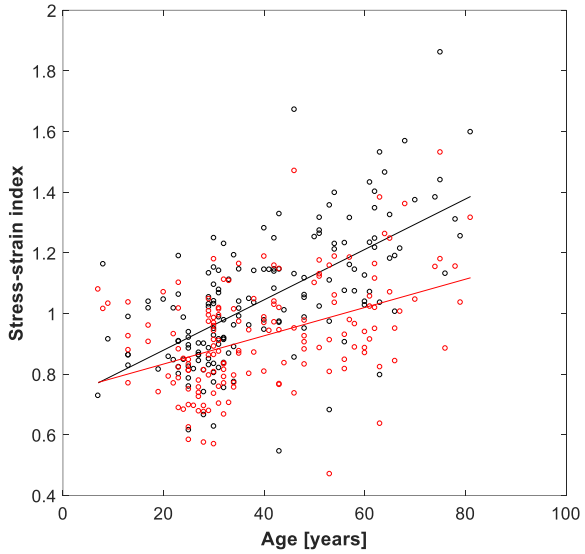

$$fSSI = 0.0083\ age + 0.71$$

$$r^2 = 0.4146$$

$$SSI = 0.0047\ age + 0.74$$

$$r^2 = 0.1905$$

(c) fIOP

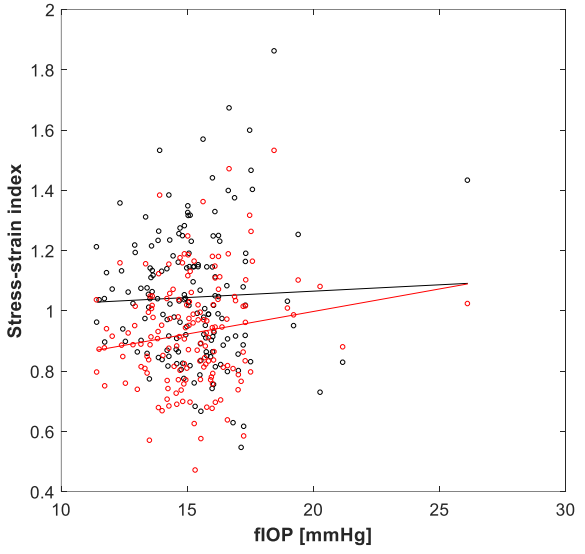

$$fSSI = 0.0042\ fIOP + 0.98$$

$$r^2 = 0.0014$$

$$SSI = 0.015\ fIOP + 0.7$$

$$r^2 = 0.0255$$

477

Figure 5 Association of the corneal material parameter fSSI with (a) CCT, (b) age, and (c) fIOP